Science Bulletin xxx (xxxx) xxx

Contents lists available at ScienceDirect

Science Bulletin

journal homepage: www.elsevier.com/locate/scib

Article

Integrated intelligent tactile system for a humanoid robot

Rongrong Bao [a,b,1], Juan Tao [a,b,1], Jing Zhao [a,b], Ming Dong [c], Jing Li [a,b], Caofeng Pan [a,b,*]

[a] CAS Center for Excellence in Nanoscience, Beijing Key Laboratory of Micro-nano Energy and Sensor, Beijing Institute of Nanoenergy and Nanosystems, Chinese Academy of Sciences, Beijing 101400, China
[b] School of Nanoscience and Engineering, University of Chinese Academy of Sciences, Beijing 100049, China
[c] Beijing Institute of Tracking and Telecommunications Technology, Beijing 100094, China

ARTICLE INFO

Article history:
Received 22 December 2022
Received in revised form 6 March 2023
Accepted 14 April 2023
Available online xxxx

Keywords:
Intelligent tactile system
Artificial tactile systems
Closed-loop feedback control
Flexibly grasp

ABSTRACT

Tactile perception is the basis of human motion. Achieving artificial tactility is one of the challenges in the fields of smart robotics and artificial intelligence (AI), because touch emulation relies on high-performance pressure sensor arrays, signal reading, information processing, and feedback control. In this paper, we report an integrated intelligent tactile system (IITS) that is integrated with a humanoid robot to achieve human-like artificial tactile perception. The IITS is a closed-loop system that includes a multi-channel tactile sensing e-skin, a data acquisition and information processing chip, and a feedback control. With customized preset values of threshold pressures, the IITS-integrated robot can flexibly grasp various objects. The IITS has potential applications in the design of prosthetic hands, space manipulators, deep-sea exploration robots, and human-robot interactions.

1. Introduction

The rapid development of artificial intelligence (AI) and its integration with robotics have extended the applications of robots from the manufacturing sector to daily life as well as healthcare [1–3]. Smart robots require various sensory systems capable of identifying complex deformations and environmental interactions. Besides visual, auditory, and olfactory sensing capabilities, tactile perception is increasingly demanded in service-oriented applications [4–6], since touch emulation necessitates the development of large-scale pressure sensor arrays with high spatial resolution, high sensitivity, and fast response. Smart robots with intelligent tactile perception can be used as care robots in the healthcare environment, collaborative robots that assist humans and augment their capabilities and safety in various fields, industrial robots that achieve higher work precision in the manufacturing ecosystem, medical rehabilitation robots that are safer and more emotional, and exploratory robots in unpredictable and inaccessible regions of the world. Thus, robots can be friendlier when interfacing among themselves, with the surroundings, and with humans, yielding richer, more productive experiences for human users.

The final objective of research on intelligent robotics is to develop robots capable of mimicking the full range of response to stimuli of the human skin as the latter plays a critical role in daily interactions of human beings. The stimuli-response mechanism of the human skin consists of three parts: information acquisition (skin), processing (brain motion control area), and transmission (nerve) [7]. This enables the humans to feel, weigh, and grasp a diverse range of objects with a right amount of force/pressure [8,9]. Based on this mechanism in the humans, the development of an intelligent robot with a complete tactile feedback closed-loop feature will require high-resolution sensor skins, algorithms for interpreting sensor information, and reliable feedback control for robots corresponding to the coupling functions of the skin, nerves, and brain [10–14]. Previous extensive efforts in this regard focused on improving the performance of sensors, such as high sensitivity [15,16], wide detection range [17,18], and high resolution [19,20], along with stretchability [21,22], multifunctionality [23,24], biodegradability [25,26], and self-healing [27,28], based on different mechanisms including piezoresistive [29,30], capacitive [4,31,32], piezoelectric [19,20,33], and triboelectric tactile sensors [34–36]. However, only few studies have been conducted on the feedback closed-loop feature because such an endeavor would necessitate a close collaboration among robotics engineers, computer and data scientists, and materials scientists. The mimicry of human skin or integration of such a capability in robots is a complex yet inspiring scientific study because future robots will need a feedback capability to perform trivial tasks for humans. To endow robots with tactile perception, the problem of the perception-feedback function in a tactile system

* Corresponding author.
E-mail address: cfpan@binn.cas.cn (C. Pan).
[1] These authors contributed equally to this work.

https://doi.org/10.1016/j.scib.2023.04.019

Please cite this article as: R. Bao, J. Tao, J. Zhao et al., Integrated intelligent tactile system for a humanoid robot, Science Bulletin, https://doi.org/10.1016/j.scib.2023.04.019

must be solved. More importantly, the performance of such a system should be evaluated over a holistic range of practical robotic tasks, such as holding a paper cup by an in-home assistant robot. Therefore, from the tactile sensor array, the multichannel signal processing circuit, to the feedback grasping controlling, we demonstrates a tactile-based approach to fine control the movements of robot, elaborately. Various fragile objects of a controlling grasping in robots and prosthetic' hand have been exhibited, providing a prospective proof of concept in future intelligent robots.

In this study, we developed an integrated intelligent tactile system (IITS) for a humanoid robot to achieve artificial tactile perception through real-time feedback control. The IITS is a closed-loop system consisting of a high-performance skin with multi-channel tactile sensors, a data acquisition/interpreting chip, and a feedback control that reads the pressure distribution across the robotic hand with a sensitivity of approximately 0.017 kPa^{-1} and a wide range of detection up to 250 kPa. Then, data acquisition and information processing are carried out simultaneously during the dynamic grasping process of the robot. Finally, once the threshold value of pressure has been exceeded, i.e., a value above which the object may be damaged, the IITS fires a stop feedback-control command to terminate the grasping process. With a suitable preset threshold value of pressure, the robot can flexibly grasp various objects including balloons, paper cups, soft cakes, and live silkworms. The IITS has potential applications in the design of prosthetic hands, personal robots, human–robot interactions, space manipulator, and deep-sea exploration robots.

2. Materials and methods

2.1. Design and fabrication of tactile sensing skin

First, the poly(vinyl alcohol) nanofibers (PVA NFs) were prepared by the electrospinning technique (Shenzhen Tong Li Tech Co. Ltd.) under the following conditions: PVA water solution with a concentration of 10 wt%, a flow rate of 0.3 mL h^{-1}, a constant potential of 11 kV, and a spinning duration of approximately 10 min. Next, a layer of Ag film was coated on the PVA NFs through magnetron sputtering (PVD75 Kurt J. Lesker) with a sputtering power of 60 W and a duration of approximately 25 min. The Ag NFs were transferred to a polyethylene terephthalate (PET) (5 cm × 5 cm) substrate by dissolving the PVA NFs in water. Ag NFs/PET flexible electrodes with a circular radius of 2.5 mm were obtained by laser cutting. For the porous dielectric layer, Ecoflex (Smooth-On 00–10) parts A and B were mixed in a weight ratio of 1:1. Subsequently, Ecoflex/NaCl-mixed silicone was obtained by mixing NaCl particles of different qualities. The mixed silicone was then poured into a 3D mold (30 mm × 60 mm × 0.8 mm) having a weight of 4.2 g to obtain a specified thickness of approximately 800 μm. After drying for 30 min at 60 °C, it was then subjected to ultrasound for 4 h at 80 °C in distilled water to remove NaCl particles and to obtain a porous dielectric layer. Finally, the capacitive sensors were directly assembled in a sandwich structure, with Ag NFs/PET acting as the top and bottom electrodes and the porous Ecoflex serving as the dielectric layer, while another thin Ecoflex film encapsulated the devices. The device fabrication process is illustrated in Fig. S1 (online).

2.2. Design of data acquisition and information processing chip

A multi-channel capacitance signal acquisition module (AD7147) was used to obtain the capacitive analog signals from the tactile skin sensors, convert them into digital signals, and transmit them to the micro control unit (MCU) via the serial peripheral interface (SPI) communication. The MCU module (PIC16F1526) was used to program the data acquisition, processing, and controlling of the tactile sensor and then relay the sensing information to the computer through the asynchronous serial port (TTL digital signal is converted to the standard RS-232 level using a MAX3232 driver chip). The computer communication module was used to store, analyze, and interpret the datasets, and push the corresponding feedback command to the robot. The real-time data of each sensor has two display modes: digital and hot spot. A cubic B-spline surface was used to fit the pressure distribution diagram of the robotic hand.

2.3. Prosthetic robotic hand controllable grasp with IITS

Twelve sensors were mounted on the surface of a prosthetic robot hand denoted as tactile sensor TS 1-TS 12, with the ground electrode upward. A latex glove was used to protect the tactile sensors. The data acquisition and information processing chips were installed on the back of the hand and inside the arm. The action of the prosthetic robot hand was controlled by an MCU in the IITS through a motion-control module, which comprised four switches. The PC was only used for real-time display of data, storage, presetting capacitance value (C_T), and triggering the action. The robotic hand system can be entirely detached from the PC and can independently complete the closed-loop action control based on the IITS.

2.4. Flexible grasp of a humanoid in-home assistive robot with IITS

The robot depicted in this work is the U05 robot purchased from Canbot, and the robot depicted in Supplementary materials (online) is the Cruzr robot purchased from Ubtech. The IITS mounted on the assistive robot was similar to that on the prosthetic robot hand. The robot's motion control is much more complex; therefore, the Wi-Fi-enabled PC was used to help the MCU control the robot's action, and store and display real-time data.

3. Results

Fig. 1 illustrates an IITS-integrated humanoid in-home assistant robot. The IITS has four parts: a high-performance, multi-channel tactile sensor skin (mimicking skin epidermis); a real-time data acquisition/interpretation chip (emulating human neural networks); back-end data processing, analysis, interpreting (mimicking the brain) and a closed-loop feedback control (mimicking the muscle). As indicated in Fig. 1, a 12-channel capacitive sensor skin is mounted on the surface or embedded in a thin layer beneath the surface of a robotic hand, providing its pressure distribution information. When the robotic hand grasps an object, such as a cup of water, a chip (AD7147) instantly acquires the datasets of the signals from the 12-channel capacitive sensors. The chip converts the analog signals into digital signals and transmits them to a microcontroller unit (MCU, PIC16F1526) or a host computer where the datasets are stored, analyzed, and interpreted. Lastly, a corresponding feedback command is sent to the robot. Meanwhile, a pressure-distribution map is simultaneously generated and demonstrated on the host computer.

For each object, there is a threshold applied pressure above which the object may be damaged during the grasping process. Therefore, an appropriate capacitance value (C_T) corresponding to the threshold pressure is determined and preset in the MCU. When the pressure is lower than the threshold, the robot receives a feedback command from the IITS to increase the grasping force. When the pressure of any sensor in the array reaches the threshold, the IITS commands the robot to terminate the grasping action, generating a controlled grasp that prevents the potential destruction of

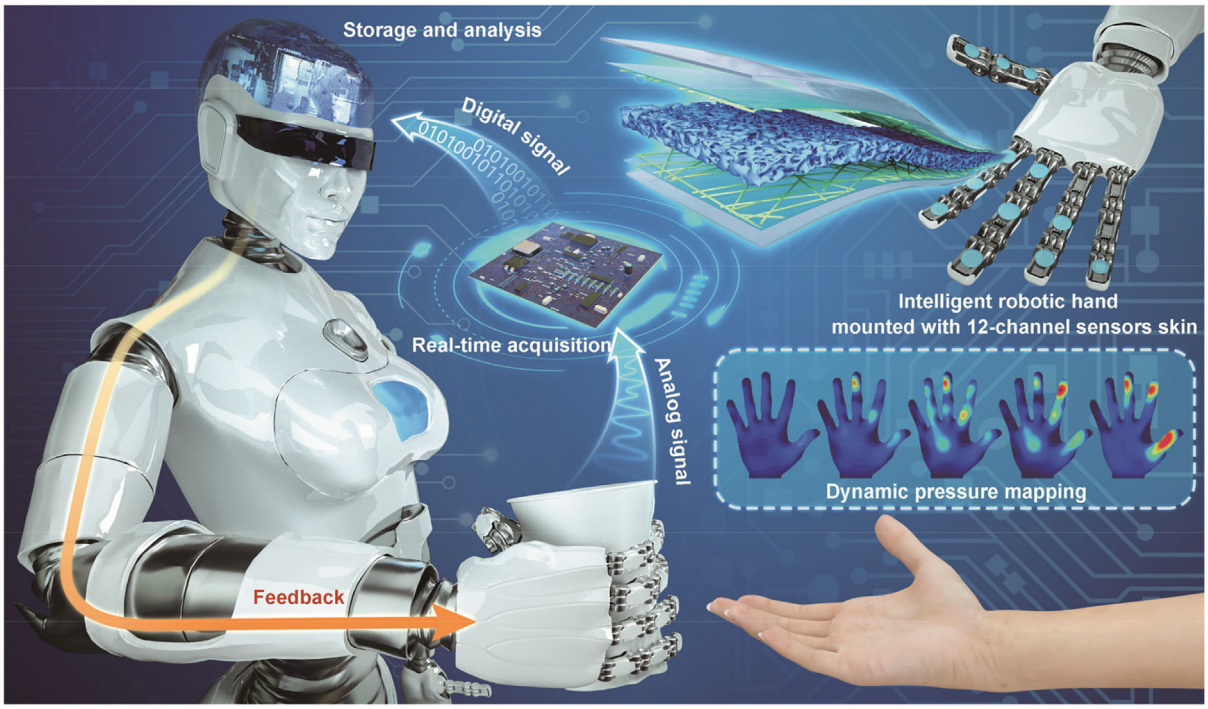

Fig. 1. Working mechanism of the IITS. IITS is composed of three parts: front-end stimulus perception based on tactile sensors array (skin-like epidermis), real-time sensor information acquisition (neural network), and back-end data processing, analysis, interpretation and closed-loop feedback control (brain).

the object. Such a closed-loop feedback control process can provide technical support for intelligent machinery and robot precise action design. Thus, because of its ability to emulate the human skin, nerves, brain, and muscles, the IITS has significance with regard to the motion feedback process in robotics or prosthesis.

Flexible tactile sensory arrays with a wide dynamic range, high resolution, and high sensitivity are the basis of IITS. As illustrated in Fig. 2a, a sandwich structure of a capacitive tactile sensory device was adopted, which is composed of a porous dielectric layer and two flexible electrode layers. The corresponding detailed fabrication process is depicted in Fig. S1 (online). An Ecoflex with a porous microstructure is used as the dielectric layer, which is fabricated by sequentially mixing and removing soluble NaCl particles into Ecoflex (Fig. S1a online). An Ag nanofiber (Ag NF) mesh on PET was used as the flexible top and bottom electrodes. The fabrication process is illustrated in Fig. S1b (online). The scanning electron microscopy (SEM) images of the porous Ecoflex and Ag NF mesh are shown in Fig. 2b and c. The porous Ecoflex has a uniform pore distribution with an average pore diameter of approximately 500 μm, while Ag NFs with an average diameter of approximately 700–800 nm possess excellent conductivity, transparency, and flexibility.

For a capacitive tactile sensor, the thickness of the dielectric layer (d_0) is reduced by an external pressure, resulting in a capacitance change. The sensitivity (S) of a capacitive tactile sensor is defined as follows

$$S = \frac{\left(\frac{C'-C_0}{C_0}\right)}{\Delta\sigma} = \frac{\frac{\Delta C}{C_0}}{\Delta\sigma}, \quad (1)$$

where σ is the applied pressure, C_0 and C' are the capacitance values of the sensor before and after the application of the external pressure. The relative change in capacitance ($\Delta C/C_0$) as a function of pressure between unstructured and porous structured Ecoflex dielectric layers with different NaCl additives measured by an LCR meter (inductance, capacitance, and resistance measurement device) is shown in Fig. 2d and e. The change exhibits an obvious linearly increasing trend in the pressure range of 0–20 and 20–100 kPa, respectively. In the low-pressure range of 0–20 kPa, the air in the porous Ecoflex dielectric layer is easily compressed under applied pressure, leading to a higher sensitivity than that in the high-pressure range of over 20 kPa. To quantitatively investigate the additive NaCl on the sensitivity of tactile sensors, we define r as the weight ratio of W_{Ecoflex} to W_{NaCl} when they are mixed. As indicated in Fig. 2d and Fig. S2d (online), the transparency of the Ecoflex dielectric layer decreases, but the sensitivity is enhanced by introducing the porous structure. The lower the r, the better is the sensitivity. The sensitivity of the porous Ecoflex dielectric layer of r = 1 can be 17 × 10^{-3} kPa^{-1} over detection range of 0–20 kPa, compared with the sensors composed of unstructured and other Ecoflex dielectric layers. According to Fig. 2f, the LCR receives response and relaxation times of approximately 125 and 250 ms, respectively, which is mostly due to the slow period of time for applying/retracting the mechanical force of a linear motor or the low readout speed of the LCR meter. The true response time of this device is expected to be much lower than 100 ms.

In addition, the tactile sensors also possess good resilience over a wide detection range of 0–250 kPa and recover quickly. The pressure responses of a tactile sensor with pressure loading and unloading are quite consistent with each other as shown in Fig. 2g. Moreover, the relative capacitance change in different external pressures is presented, demonstrating the feasibility of perceiving different external pressures over a wide detection range (Fig. 2h). Further, the tactile sensor has good stability over approximately 2000 cycles of loading and unloading of a pressure of 100 kPa, validating its use in practical applications (Fig. 2i). The insets are enlarged views of the 50th–60th and 1990th–1910th cycles, where the capacitance variation remains almost the same, demonstrating the high stability of the tactile sensor skin.

A real-time data acquisition and sensor information processing chip was designed, as shown in Fig. 3. This chip is the core of the IITS that helps realize controlled flexible feedback grasping. As

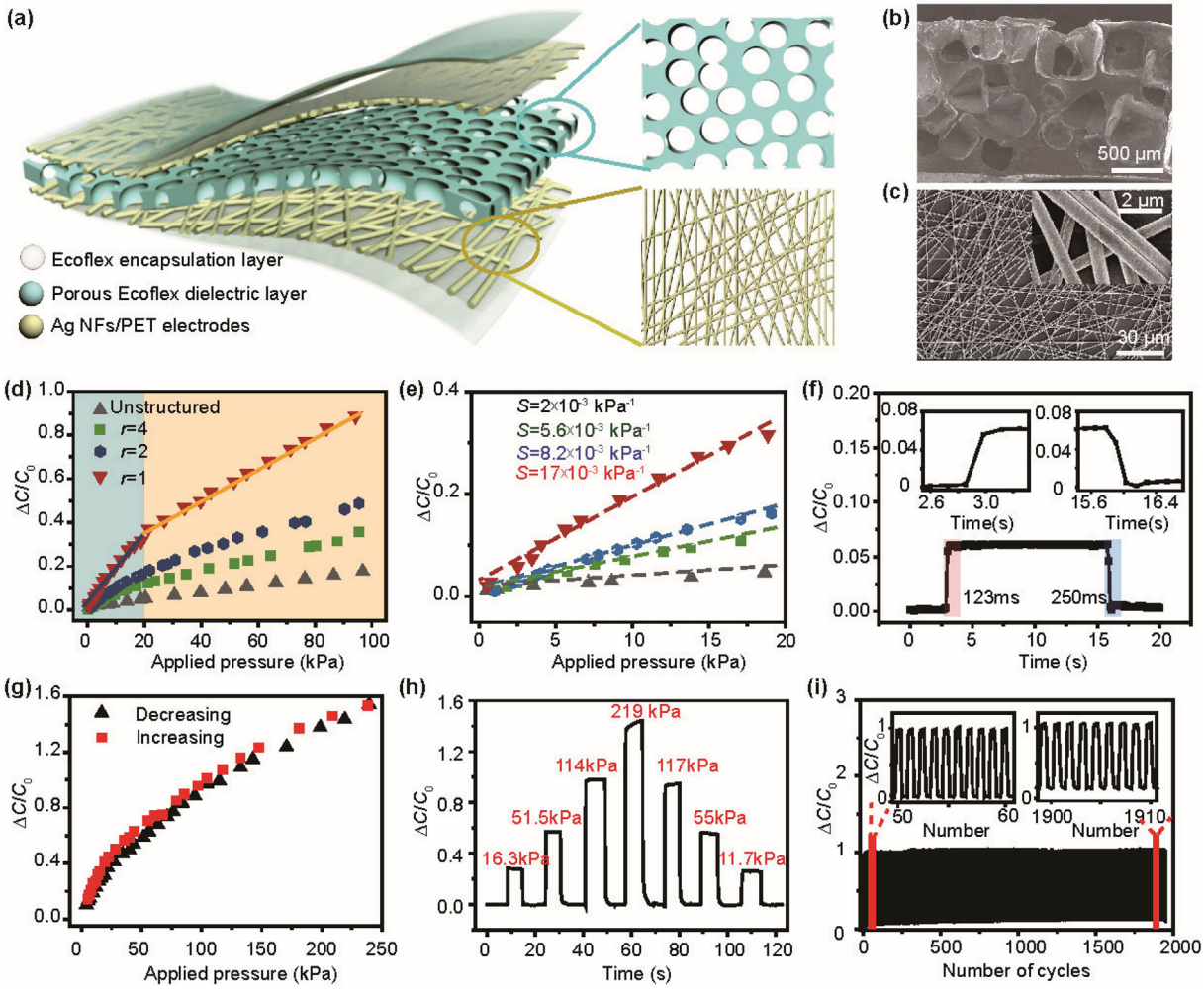

Fig. 2. Design, fabrication, and characterizations of the tactile sensing skin. (a) The sandwich structure of a capacitive tactile sensory device consisting of flexible electrodes based on Ag NFs/PET, a porous Ecoflex dielectric layer, and a thin layer of encapsulation. (b) SEM image of the porous dielectric layer cross section, with an average pore diameter of approximately 500 μm. (c) SEM image of Ag NFs with a width of approximately 700–800 nm. (d) Performance comparison of tactile sensors with different $W_{Ecoflex}$ to W_{NaCl} mixing mass ratios. (e) Magnified sensitivity curves over a detection range of 0–20 kPa. (f) Response and relaxation times of the tactile sensor. (g) Resilience of the tactile sensor over a wide detection range of 0–250 kPa. (h) Relative change in capacitance curves for different applied pressures. (i) Stability of the tactile sensor over approximately 2000 cycles under an external pressure of 100 kPa.

shown in Fig. 3a, the chip has three parts: a multi-channel capacitance signal acquisition module, an MCU module, and a personal computer (PC) communication module. The first module is used to obtain the capacitive analog signals from the tactile skin sensors array (Fig. 3b), convert them into digital signals, and transmit the signals to the MCU via the serial peripheral interface (SPI). The MCU module is used to program the data acquisition, processing, and control of the tactile sensors, and relay the sensory information to the PC through an asynchronous serial port. The PC communication module is used to store, analyze, and interpret the datasets, and transmit the corresponding feedback command to the robot. The detailed hardware block diagram of the grasp perception system is illustrated as a flow chart in Fig. 3a and Fig. S3 (online). It contains the schematic diagram of the grasping perception system and the main program. The prosthetic hand and robot's hand are combined with IITS, with the optical photograph illustrated in Fig. 3c and detailed sensors distribution in Fig. S4 (online). Fig. 3d compares two ΔC-pressure curves of one tactile sensor obtained via an LCR meter (black dots) and our IITS data acquisition chip (red dots), respectively. As illustrated in the figure, the two ΔC-pressure curves have a similar trend with only a small baseline shift, which may be caused by different background interferences of the electrical circuit. This means the chip is highly accurate and can be used in our IITS research.

It should be noted that the feedback action of the entire IITS system can work coherently with the MCU, whereas the PC is only used for data storage, presetting the C_T, and firing the command of the initial grasp. When the preset threshold pressure values for the MCU are set in advance, and one of the tactile sensors is used as the action switch, the smart robotic hand works completely independent of the PC. Compared with the robotic hand, which is demonstrated in Figs. 4 and 5, the robot's motion control (Fig. 6) is more complex. Therefore, the PC can be used to help the MCU control the grasping action through Wi-Fi. If the robot's CPU can be programmed and integrated with the IITS, its motion control can achieve a closed loop even without a PC.

Before it was used to control the grasping of an object, the IITS data acquisition chip was used to study the mechanical properties of a few objects with different characteristics, including a balloon, a paper cup, a cake, bayberries, and an egg, to derive their threshold pressures σ_T, and thus the threshold ΔC_T (Fig. 4a). The pressure and the corresponding capacitance change of these objects were investigated iteratively. It was observed from these investigations that a balloon does not deform greatly unless the applied pressure is

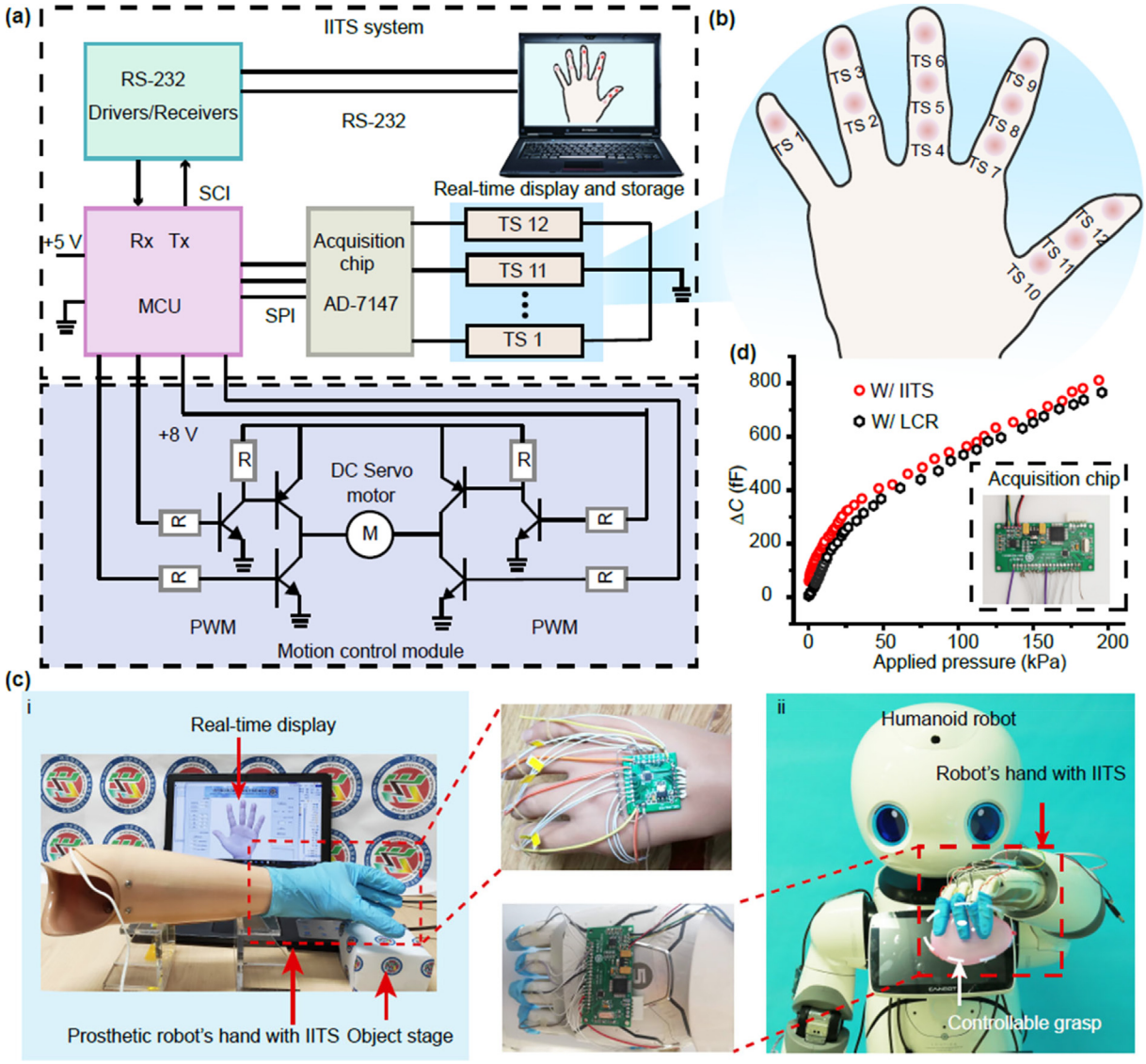

Fig. 3. Design of a data acquisition and information processing chip. (a) Schematic of chip with three parts: a multi-channel capacitance signal acquisition module, an MCU module, and a computer communication module. (b) The distribution of twelve tactile sensors (noted as TS 1-TS 12) on a robotic hand. (c) Photographs of two typical types of robotic hands with IITS. A prosthetic robotic hand (i), and a humanoid robotic hand (ii). (d) Two ΔC-pressure curves of the same tactile sensor, one obtained via an LCR meter (black dots) and the other via the IITS data acquisition chip (red dots).

higher than 2 kPa. On the other hand, paper cups, cakes, and bayberries can bear a higher threshold pressure of approximately 10 kPa before getting damaged. As a hard object with a structure that can distribute pressure evenly, eggs can be kept undamaged under a pressure of more than 15 kPa without fast impact. Based on these important data, the corresponding C_T can be obtained and then be preset in the MCU so that the robot can perfectly flexibly grasp these objects without any damage.

Since it can endure a wide range of pressure without being damaged, the balloon was chosen to demonstrate how the IITS works with a different preset C_T. Twelve sensors were mounted on the surface of a prosthetic robotic hand noted as tactile sensor TS 1–TS 12 (Fig. 3b). In a typical grasping process with IITS controlling, firstly, the host PC transmits the C_T value and fires the start command to the MCU. Then, the robotic hand moves to touch the target object causing the capacitance of the sensors to change. Then, the capacitance signal acquisition module obtains the capacitive analog signals, and converts them to digital signals, which it then transmits to the MCU. Finally, the MCU decides whether to send a stop command to the robotic hand motor by comparing the pressure of any of the 12-channel sensors with the threshold C_T. This produces a controllable grasp, avoiding the destruction of the object. In the investigation of grasping a balloon, the maximum pressure has always occurred in the tactile sensor mounted on the index fingertip, which is TS 9. Since the IITS uses the highest pressure of sensors in the array to trigger the stop decision, we plot the capacitance-time (ΔC-t) curves of TS 9 under ten different preset C_T (Fig. 4b). Since a balloon is a soft object and can suffer a range of applied pressures until failure, a set of C_T was taken to test the IITS system. As indicated in the figure, the motor of the robotic hand stops when the capacitance of TS 9 reaches the preset C_T in all the ten cases. Fig. 4c (i) illustrates a set of photographs of the balloon at different stages of the grasping process and its corresponding C_T values (C_T 1–C_T 10). The figure illustrates the gradual deformation of the balloon with an increase of the applied pressure due to the preset threshold increasing from C_T 1 to C_T 10. The ten different pressure distributions corresponding to C_T 1 to C_T 10 are shown in Fig. 4c (ii), which are consistent with the trend of

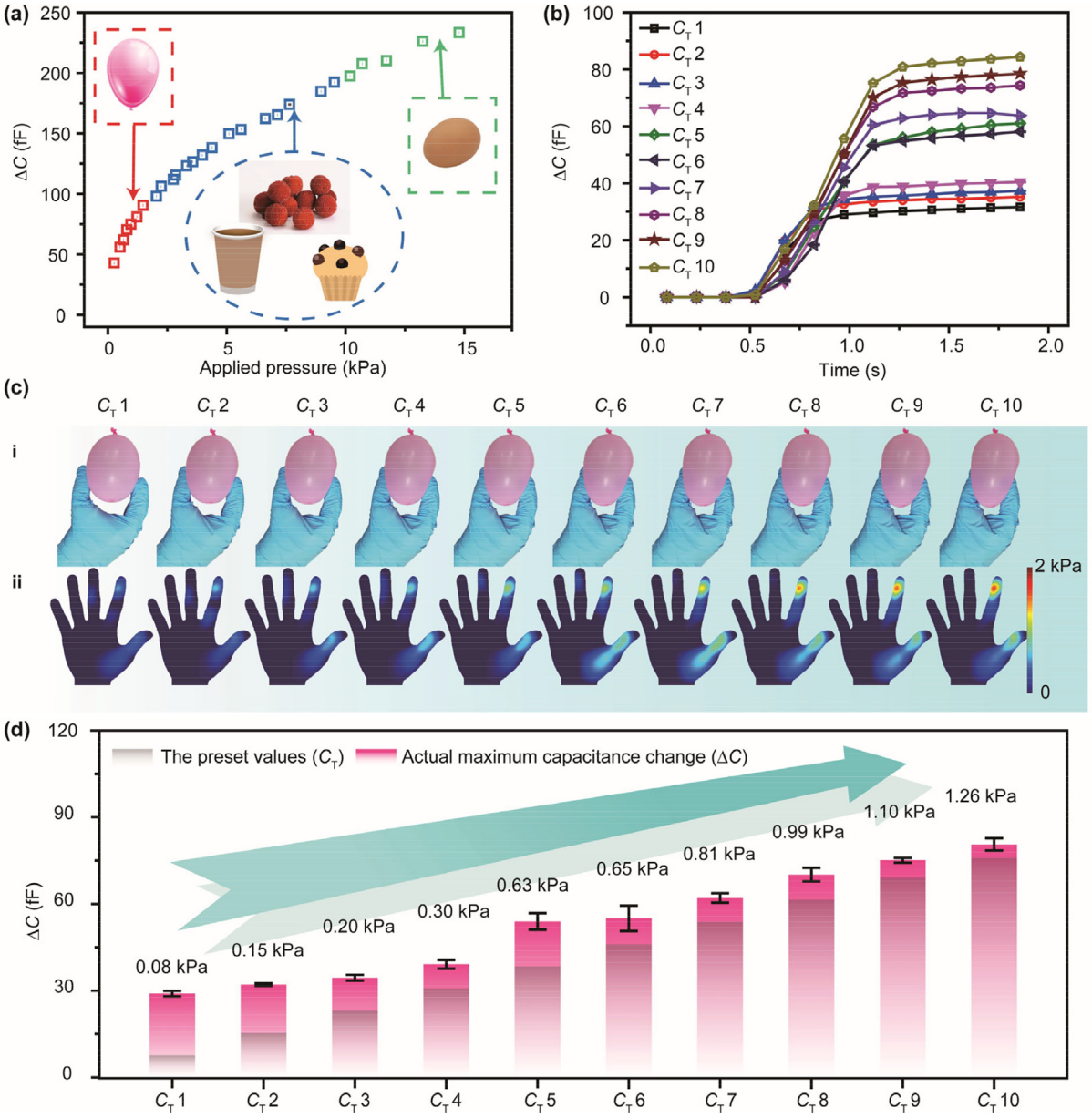

Fig. 4. Controlled grasping of a balloon by IITS. (a) The threshold pressure σ_T and the threshold ΔC_T of different objects by IITS chip. (b) The capacitance-time (ΔC-t) curves of the tactile sensor TS 9 with ten different preset C_T. (c) The photographs of the balloon deformation (i), and corresponding pressure distributions comparison when the C_T increases from C_T 1 to C_T 10 (ii). (d) The deviation between the experimental ΔC at which the robotic hand stops and the preset C_T.

the entire experimental process. The balloon deformation and the pressure of the tactile sensor increase with the preset C_T. The ΔC-t curves of all sensors of the robotic hand at three different typical C_T (C_T 1, C_T 5, and C_T 10) values are given in Fig. S4 (online), with the corresponding optical photographs, simultaneously.

We found a small deviation between the actual maximum capacitance change (ΔC) and the preset values (C_T), which may have been caused by the delays of the entire system (the response delay of sensors, the delay of data acquisition system, and the delay of motor). As shown in Fig. 4d, the higher the preset pressure value in the experiment, the smaller the gap between the maximum pressure and the preset C_T when the robotic hand stops. This is because of the high reaction force on the robotic hand due to the significant deformation of the balloon, which helps reduce the motor-stop delay.

A paper cup has a harder surface and could undergo an irreversible deformation, compared with a balloon. In this section, the controlled grasp experiment of a paper cup and a live silkworm is detailed to verify the sensitivity and reliability of the IITS. The paper cup grasp-action with and without the IITS can be divided into four steps, according to the capacitance change of the 12-channel tactile sensor skin in Fig. 5a. Without the IITS, as shown in Fig. 5a (A1), an extremely high threshold C_T of approximately 600.0 fF was set in the MCU, which will never be reached. In step (i), the fingers of the robotic hand do not touch the cup, which means the skin has no signal output change in capacitance. In step (ii), the fingers start to touch the paper cup, inducing a slight deformation. In this step, the pressure of the sensors touching the cup (TS 3, TS 6, TS 9, and TS 11) increases rapidly, as highlighted in Fig. 5b. This process lasts for a short period of time because the pressure applied on the paper cup quickly reaches the IITS threshold pressure σ_T. In step (iii), the decreasing capacitance indicates that the cup has been irreversibly deformed. In the last step (step (iv)), as the robotic hand continues to grasp, the paper cup is totally

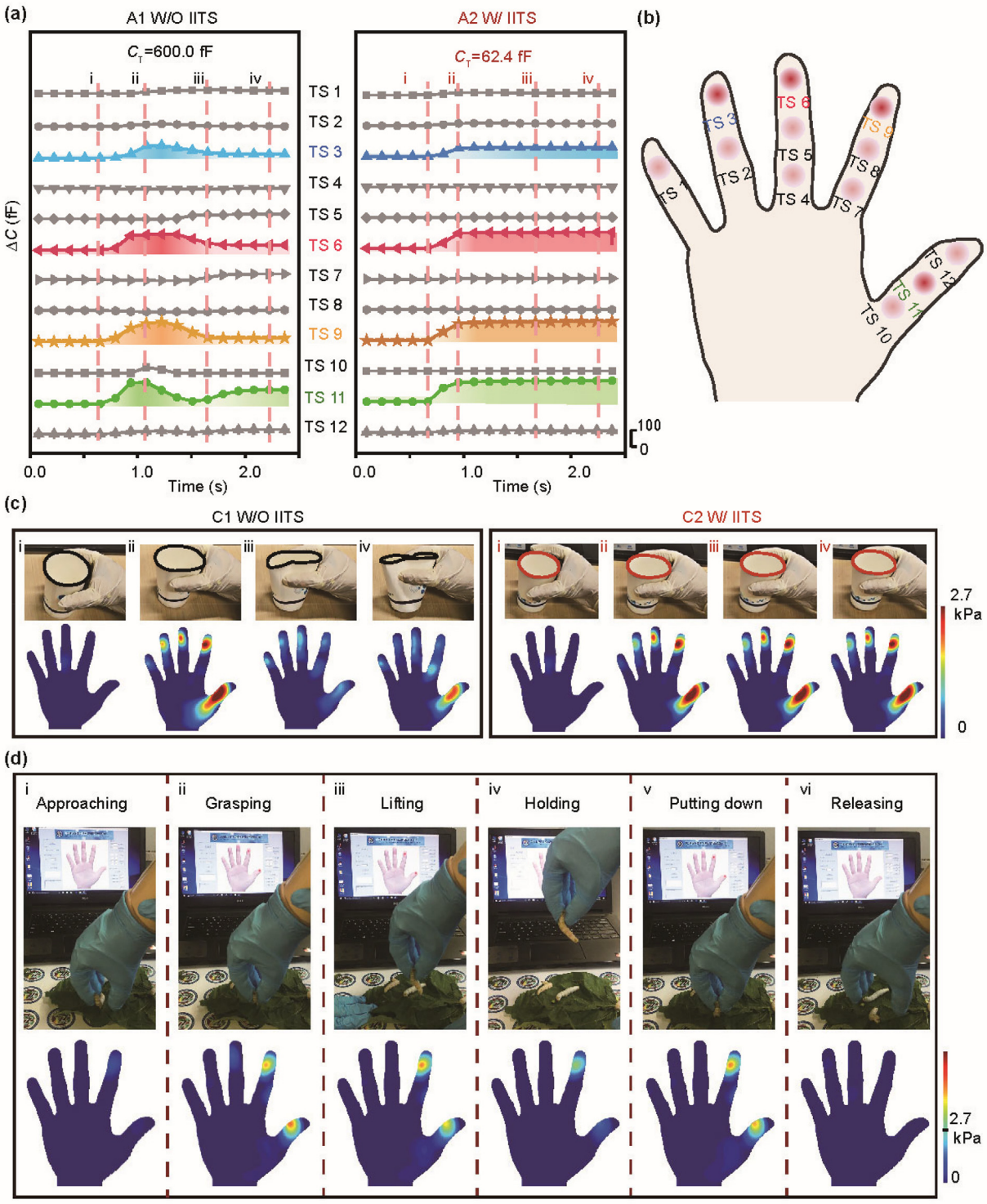

Fig. 5. Controlled grasping of a paper cup and a silkworm. (a) The paper cup grasping process without and with the IITS. (b) Illustration of four dominant tactile sensors (TS 3, TS 6, TS 9, and TS 11) during the paper cup grasp process. (c) The pressure distributions in two processes of grabbing a cup with (red) and without (black) the IITS-enabled control. (d) The flexible grasping of a live silkworm with a proper threshold CT by IITS, with the following six steps: approaching (i), grasping (ii), lifting (iii), holding (iv), putting down (v), releasing (vi).

deformed, with the sides being pushed in until they come in contact with the opposite sides, at which the pressure measured by the sensor (such as TS 11 on thumb) increases abruptly. With the IITS, a proper threshold C_T was approximately 62.4 fF. The entire grasping action terminated at the end of step (ii) when the highest capacitance change reached the preset C_T. Moreover, the sensor signals also stabilized in steps (ii)–(iv) without any further increase, as illustrated in Fig. 5a (A2). The experimental data are in accordance with the grasping process of the paper cup. Because the pressure applied on the paper cup rapidly reaches the IITS threshold pressure σ_T, the process from touching to breaking the paper cup occurs in a significantly short duration (step (ii)), and

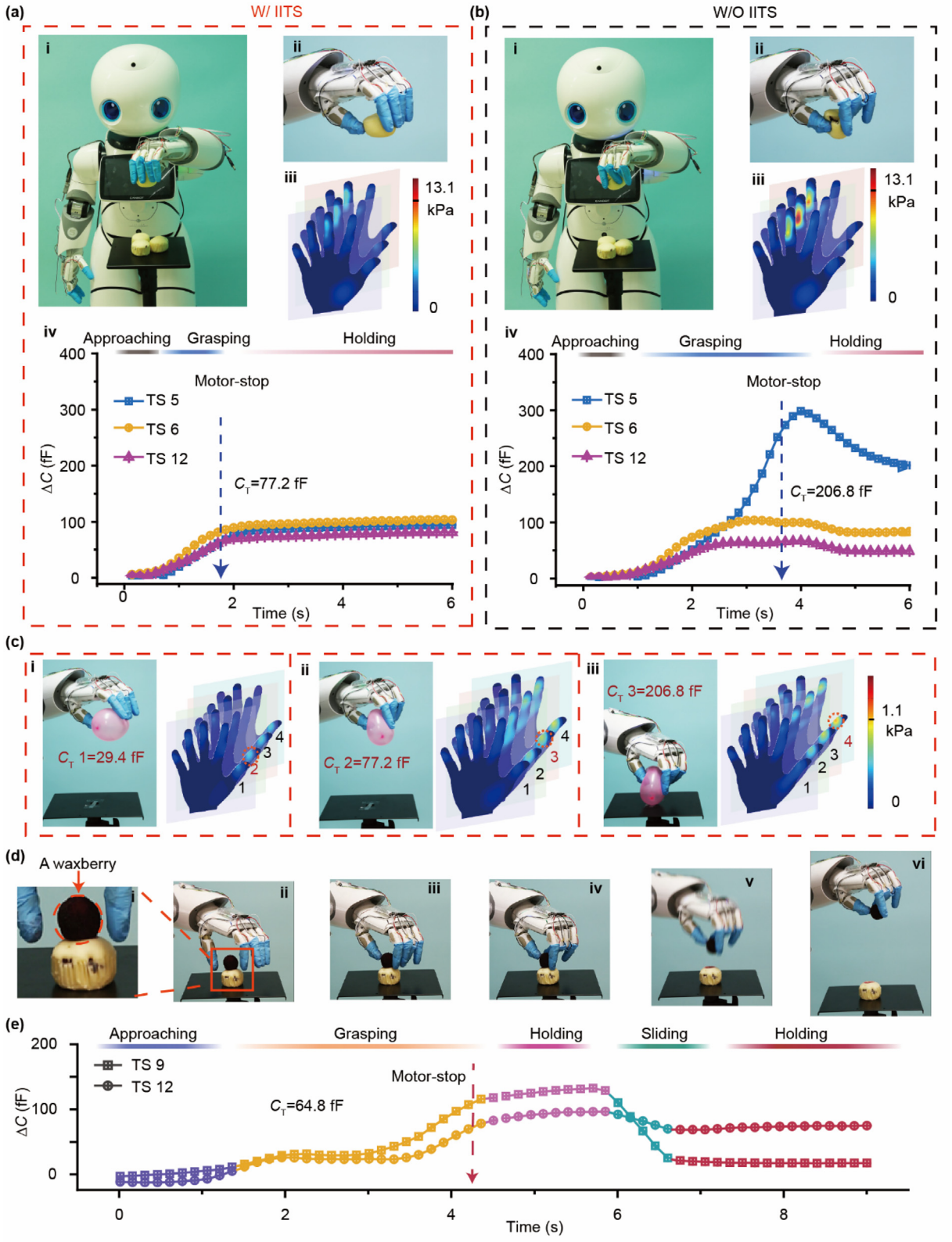

Fig. 6. Flexible grasping of a Robot by IITS. (a) Controlled grasping of cake with IITS and (b) uncontrolled grasping of a cake without IITS: the front optical photograph of the robot (i), enlarged image focusing on the grasping of cake (ii), the pressure distribution of the process (iii), and the ΔC-t curves of TS 5, TS 6 and TS 12 (iv). (c) IITS-controlled grasping of balloons with different C_T values from 29.4 (i), 77.2 (ii), to 206.9 (iii) fF. (d) A set of optical photographs and (e) the capacitance–time curves of TS 9 and TS 12 in the entire process of picking up a waxberry with the IITS.

this demonstrates the sensitivity and reliability of the IITS. A set of photographs comparing the pressure distribution evolution trends of the grasping process by the robotic hand with and without the IITS is listed in Fig. 5c (C1) and Movie S1 (online). The figure and the movie clearly show that the robot can flexibly grasp a paper cup with the IITS.

As shown in Fig. 5d, we also demonstrated the flexible grasping of a live silkworm by the robotic hand with the IITS, with a proper threshold C_T of approximately 92.2 fF set in the MCU. The pressure corresponding to C_T of 92.2 fF (pressure of approximately 2.5 KPa), which will not hurt the silkworm in this test, can be obtained by iterative grasping experiments and machine learning. When flexibly grasping a silkworm, we found that the capacitances of the tactile sensors on the index and thumb fingertips (TS 9 and TS 12) were the highest, and they reached the threshold C_T when the MCU pushed a stop feedback command to the robotic hand. The IITS has high sensitivity, with which it is possible to detect even the movement of the silkworm when it being grasped. As observed from the pressure distribution of the robotic hand, the capacitances of tactile sensors on the index (TS 9) and thumb (TS 12) fingertips decrease with the swinging of the silkworm, and then increase after the silkworm makes contact with the desktop again, according to the dynamic pressure mapping in Fig. 5d (i) to (vi). When the silkworm was released by the robotic hand, it was still alive without injury, as shown in Fig. 5d (vi) and Movie S2 (online).

The IITS can be applied to more complex mechanical devices to complete precise tasks with a tactile feeling. For example, humanoid in-home assistive healthcare robots for providing physical comfort to patients, collaborative robots to assist humans and augment their capabilities and safety in various fields, industrial robots that achieve higher work precision in the manufacturing ecosystem, medical rehabilitation robots that are safer and friendlier, and exploratory robots in unpredictable and inaccessible regions of the world. Controlling a robot's motion is much more complex than controlling a single robotic hand. Therefore, a PC was used to help the MCU control the robot's action, and display real-time data and storage through Wi-Fi signals. An appropriate C_T corresponding to the threshold pressure was set before the robot began grasping the target objects. When the pressure is lower than the threshold (i.e., the ΔC is smaller than the C_T), the robot gets a feedback command from the IITS to increase the applied grasping force. When the pressure of any 12-channel sensor in the array reaches the threshold, the IITS commands the robot to cease the grasping motion, and the arm to pick up the object, yielding a controlled grasping motion that prevents damage to the object. In this work, we demonstrated the flexible grasping of cake (Fig. 6a and Movie S3 online), balloon (Fig. 6c), and waxberry (Fig. 6d) with a humanoid in-home assistant robot. A robot with IITS can flexibly accurately grasp the cake without causing damage (Fig. 6a (i)), if the appropriate C_T value is set. Fig. 6a (ii) is an enlarged view of the robot arm with a focus on the flexible grasping of the cake; the action does not damage the cake. The pressure distribution during this process of flexible grasping is shown in Fig. 6a (iii). The figure shows the tactile sensors TS 5, TS 6, and TS 12 as having endured the largest pressure among all sensors. The ΔC-t curves of tactile sensors TS 5, TS 6, and TS 12 are listed in Fig. 6a (iv). These curves clearly indicate that the IITS fires a feedback command to terminate the grasping action when the capacitance reaches the preset threshold (C_T) value of 77.2 fF. After that, the pressure on the sensors remains constant.

A contradictory trend is observed with the uncontrollable grasping of cake (Fig. 6b). The uncontrollable grasp is a result of setting a much higher C_T than the cake can endure. In this study, a C_T of 206.8 fF was used, which is much higher than a piece of cake can withstand. The robot crumbles the cake (Fig. 6b (ii)). The pressure distribution of the grasping process is illustrated in Fig. 6b (iii). The pressure of the tactile sensors is much higher than the pressure during the flexible grasp, which is shown in Fig. 6a (iii). The curves of tactile sensors TS 5, TS 6, and TS 12 in this uncontrolled process are plotted in Fig. 6b (iv), which are totally different from those in Fig. 6a (iv). It is obvious that the robot does not stop until ΔC reaches 206.80 fF. In the process, the pressure value of the sensors increases significantly, and then decreases as the cake begins to crumble. In the uncontrolled process, the maximum pressure on the robot's finger (TS 5) is significantly higher than the one in the controlled process.

We also demonstrated the IITS-enabled controlled grasping of balloons with different C_T values. As shown in Fig. 6c (i)–(iii), as the preset C_T values increase from 29.4 to 77.2 to 206.8 fF, the deformation of the balloon varies from no deformation to minor compression, and finally large deformation. Since the balloon is a soft object, the maximum pressure does not reach the preset 206.80 fF in Fig. 6c (iii). Thus, the robot does not perform the subsequent action of lifting the arm and the balloon. This action will commence only if the IITS detects a breach of the threshold value.

The IITS can also control the robot to pick up tiny objects like waxberry, which has a diameter of approximately 25 mm. Fig. 6d and e illustrate the entire pick-up process and the ΔC-t curve obtained by the IITS system. Two videos in Supplementary materials (online) demonstrate the grasping of cake by a robot, comparing the difference between the process with (Movie S3 online) and without IITS (Movie S4 online) feedback control.

We performed an experiment on a second humanoid in-home assistant robot from another manufacturer, which also realizes the control of robot action (Fig. S5 online). The robot was designed to hold a balloon with two arms instead of one, because the fingers of this robot are too short to grasp objects. We used the IITS system to measure the pressure on each fingertip of the robot's hands and fire a stop feedback command when the measured pressure reaches the preset threshold C_T. In this process, the pressure on each finger increased as the deformation of the balloon increased. Thus, different threshold C_T values can be used to obtain the desired deformation of balloon.

4. Discussion and conclusion

During the grasping process, each object has a threshold pressure it can withstand, exceeding which will damage the object. In the IITS, the threshold pressure is preset to the MCU through the ΔC value according to the ΔC-σ plots in Fig. 4a. We found that C_T were slightly modified by the system delay, including the delay of sensors (much less than 100 ms response time), the delay of data acquisition and information processing (~150 ms), and the delay of the motor. Thus, the value of C_T input to the MCU may be smaller than the actual value, and the relationship between C_T and $\Delta\sigma_T$ can be expressed as follows

$$C_T = S \times \Delta\sigma_T \times a \times C_0, \quad (2)$$

where $\Delta\sigma_T$ is the threshold pressure and S is the sensitivity parameter of the sensor, a is the delay factor ranging from 0 to 1, which is mainly affected by the material, weight, roughness, and shape of the object. Firstly, the hardness of material is the most crucial factor. The σ_T of soft objects is low and is close to the nonlinear region of ΔC-σ curve. Therefore, to prevent soft objects from being damaged, a smaller C_T is preferred. For example, as indicated in Fig. 4d, the preset C_T deviates from the true pressure after the termination command is fired in the four experiments (C_T 1–C_T 4). Secondly, the roughness of an object determines the ease with which the object could slip when grasped. The a of rough objects can be set to a small value, while that of smooth objects requires a large value. Thirdly, heavy objects also need a larger a to avoid sliding. Fourthly, robotic hands are not as flexible as human hands, and it is difficult to grasp a small or sharp object. Moreover, the sensor's sensitivity decreases under non-uniform pressure. Therefore, in such cases, it is important to choose an appropriate a through a set of experiments. Finally, to handle fragile objects such as eggs, the robot's grasp speed should also be considered for a. Eggs can

endure a high static pressure, but they easily break when hit by a sharp or hard object.

The study of multi-modal sensing of intelligent tactile perception and other senses is germane to the simulation of human actions, such as the study of a combination of artificial tactility and vision, which can enable the robot to automatically identify the position, material, and shape of the object to be grasped. For instance, when grasping an object, the robots can perceive and judge the object initially, and then a proper grasping pressure is utilized to get a feedback-grasping for the object. Relying on the integration of recognition of objects and perceiving of grasping threshold, which both could be in virtue of advanced algorithm based on numerous data sets, this IITS can step forward to "highly intelligent", imitating of human grasping capability authentically.

In conclusion, an IITS was designed based on a flexible porous pressure sensor with a sensitivity of 0.017 kPa^{-1}, a wide range of detection pressure of 250 kPa, a real-time sensor for information acquisition/interpretation, and a closed-loop feedback control. The IITS can achieve real-time tactile sensing and grasping control of smart robotic hands. Preset values of C_T for the IITS were obtained by considering the hardness, surface roughness, and brittleness of the object to be grasped. By comparing the real-time pressure distribution on the robotic hand with the preset C_T, the IITS decides when to stop grasping and lifting an object and grasps soft objects (such as paper cups, cakes, balloons, and live silkworms) without damaging them. The system simulates the tactile and motion feedback process of the human skin, nerves, and muscle, and can be directly attached to the surface of existing intelligent machinery. Thus, it offers the advantages of compactness and easy installation without forcing any major changes to the mechanical structure. Therefore, this system may have extensive applications for collaborative robots, industrial robots, medical rehabilitation robots, and exploratory robots including space and deep-sea robots. Thus, the IITS may spur technological innovations in the field of intelligent machinery and robotics.

Conflict of interest

The authors declare that they have no conflict of interest.

Acknowledgments

This work was supported by the National Key R&D program of China (2021YFB3200302 and 2021YFB3200304), Beijing Natural Science Foundation (L223006, Z180011, and 2222088), Shenzhen Science and Technology Program (KQTD20170810105439418), the National Natural Science Foundation of China (52125205, U20A20166, and 52192614), and the Fundamental Research Funds for the Central Universities.

Author contributions

Rongrong Bao and Caofeng Pan proposed the experimental concept of the intelligent tactile system for robots. Rongrong Bao and Juan Tao fabricated and characterized the capacitive sensors. Rongrong Bao and Ming Dong designed the data acquisition and feedback system. Rongrong Bao developed the intelligent robotic hand and the other two robotic hands. Rongrong Bao, Juan Tao, and Jing Zhao performed the grasp experiments of different objects and recorded them on videos. Rongrong Bao, Juan Tao, and Caofeng Pan performed all data collection and analyses. Rongrong Bao developed the simulations of pressure distribution on the palm. Rongrong Bao and Caofeng Pan drafted the manuscript. All authors discussed the results and commented on the manuscript.

Appendix A. Supplementary materials

Supplementary materials to this article can be found online at https://doi.org/10.1016/j.scib.2023.04.019.

References

[1] Rus D, Tolley MT. Design, fabrication and control of soft robots. Nature 2015;521:467–75.
[2] Peters BS, Armijo PR, Krause C, et al. Review of emerging surgical robotic technology. Surg Endosc 2018;32:1636–55.
[3] Massari L, Fransvea G, D'Abbraccio J, et al. Functional mimicry of ruffini receptors with fibre bragg gratings and deep neural networks enables a bio-inspired large-area tactile-sensitive skin. Nat Mach Intell 2022;4:425–35.
[4] Boutry CM, Negre M, Jorda M, et al. A hierarchically patterned, bioinspired e-skin able to detect the direction of applied pressure for robotics. Sci Robot 2018;3:eaau6914.
[5] Sundaram S, Kellnhofer P, Li YZ, et al. Learning the signatures of the human grasp using a scalable tactile glove. Nature 2019;569:698–702.
[6] Georgarakis AM, Xiloyannis M, Wolf P, et al. A textile exomuscle that assists the shoulder during functional movements for everyday life. Nat Mach Intell 2022;4:574–82.
[7] Shih B, Shah D, Li J, et al. Electronic skins and machine learning for intelligent soft robots. Sci Robot 2020;5:eaaz9239.
[8] Kellmeyer P, Mueller O, Feingold-Polak R, et al. Social robots in rehabilitation: a question of trust. Sci Robot 2018;3:eaat1587.
[9] Sun H, Kuchenbecker KJ, Martius G. A soft thumb-sized vision-based sensor with accurate all-round force perception. Nat Mach Intell 2022;4:135–45.
[10] Wang C, Pan C, Wang ZL. Electronic skin for closed-loop systems. ACS Nano 2019;13:12287–93.
[11] Chortos A, Liu J, Bao Z. Pursuing prosthetic electronic skin. Nat Mater 2016;15:937–50.
[12] Bartolozzi C, Natale L, Nori F, et al. Robots with a sense of touch. Nat Mater 2016;15:921–5.
[13] Wen F, Zhang Z, He T, et al. AI enabled sign language recognition and VR space bidirectional communication using triboelectric smart glove. Nat Commun 2021;12:5378.
[14] Zhu M, Sun Z, Lee C. Soft modular glove with multimodal sensing and augmented haptic feedback enabled by materials' multifunctionalities. ACS Nano 2022;16:14097–110.
[15] Li J, Bao R, Tao J, et al. Visually aided tactile enhancement system based on ultrathin highly sensitive crack-based strain sensors. Appl Phys Rev 2020;7:e011404.
[16] He J, Xiao P, Lu W, et al. A universal high accuracy wearable pulse monitoring system via high sensitivity and large linearity graphene pressure sensor. Nano Energy 2019;59:422–33.
[17] Wang X, Que M, Chen M, et al. Full dynamic-range pressure sensor matrix based on optical and electrical dual-mode sensing. Adv Mater 2017;29:e201605817.
[18] Bai1 N, Wang L, Wang Q, et al. Graded intrafillable architecture-based iontronic pressure sensor with ultra-broad-range high sensitivity. Nat Commun 2020;11:209.
[19] Pan C, Dong L, Zhu G, et al. High-resolution electroluminescent imaging of pressure distribution using a piezoelectric nanowire LED array. Nat Photon 2013;7:752–8.
[20] Peng Y, Que M, Lee HE, et al. Achieving high-resolution pressure mapping via flexible GaN/ZnO nanowire LEDs array by piezo-phototronic effect. Nano Energy 2019;58:633–40.
[21] Wang X, Zhang Y, Zhang X, et al. A highly stretchable transparent self-powered triboelectric tactile sensor with metallized nanofibers for wearable electronics. Adv Mater 2018;30:1706738.
[22] Jang KI, Chung HU, Xu S, et al. Soft network composite materials with deterministic and bio-inspired designs. Nat Commun 2015;6:6566.
[23] Hua Q, Sun J, Liu H, et al. Skin-inspired highly stretchable and conformable matrix networks for multifunctional sensing. Nat Commun 2018;9:244.
[24] Sun BH, McCay RN, Goswami S, et al. Gas-permeable, multifunctional on-skin electronics based on laser-induced porous graphene and sugar-templated elastomer sponges. Adv Mater 2018;30:e1804327.
[25] Boutry CM, Beker L, Kaizawa Y, et al. Biodegradable and flexible arterial-pulse sensor for the wireless monitoring of blood flow. Nat Biomed Eng 2019;3:47–57.
[26] Feig VR, Tran H, Bao Z. Biodegradable polymeric materials in degradable electronic devices. ACS Cent Sci 2018;4:337–48.
[27] Sun J, Pu X, Liu M, et al. Self-healable, stretchable, transparent triboelectric nanogenerators as soft power sources. ACS Nano 2018;12:6147–55.
[28] Deng J, Kuang X, Liu R, et al. Vitrimer elastomer-based jigsaw puzzle-like healable triboelectric nanogenerator for self-powered wearable electronics. Adv Mater 2018;30:e1705918.
[29] Chen G, Matsuhisa N, Liu ZY, et al. Plasticizing silk protein for on-skin stretchable electrodes. Adv Mater 2018;30:e1800129.
[30] Choong CL, Shim MB, Lee BS, et al. Highly stretchable resistive pressure sensors using a conductive elastomeric composite on a micropyramid array. Adv Mater 2014;26:3451–8.

[31] Ruth SRA, Beker L, Tran H, et al. Rational design of capacitive pressure sensors based on pyramidal microstructures for specialized monitoring of biosignals. Adv Funct Mater 2020;30:1903100.
[32] Zhao X, Hua Q, Yu R, et al. Flexible, stretchable and wearable multifunctional sensor array as artificial electronic skin for static and dynamic strain mapping. Adv Electron Mater 2015;1:1500142.
[33] Bao R, Wang C, Dong L, et al. Flexible and controllable piezo-phototronic pressure mapping sensor matrix by ZnO NW/P-polymer LED array. Adv Electron Mater 2015;25:2884–91.
[34] Wen F, Sun Z, He T, et al. Machine learning glove using self-powered conductive superhydrophobic triboelectric textile for gesture recognition in VR/AR applications. Adv Sci 2020;7:2000261.
[35] Tao J, Bao R, Wang X, et al. Self-powered tactile sensor array systems based on the triboelectric effect. Adv Funct Mater 2019;29:1806379.
[36] Liu D, Yin X, Guo H, et al. A constant current triboelectric nanogenerator arising from electrostatic breakdown. Sci Adv 2019;5:eaav6437.

Rongrong Bao received her B.S. degree from Tianjin University in 2007 and Ph.D. degree from Technical Institute of Physics and Chemistry, Chinese Academy of Sciences (CAS) in 2012. She had been a postdoc fellow in the same institute. She has been an associate professor in the group of Prof. Caofeng Pan at Beijing Institute of Nanoenergy and Nanosystems, CAS since 2016. Her main research interest focuses on the fields of the production and characterization of organic–inorganic composite nano-devices and flexible pressure sensor.

Juan Tao received her Ph.D. degree (2020) at Institute of Semiconductors, CAS. She did her postdoctoral research at Shenzhen University in 2020–2022. Then, she worked at Jiashan Fudan Institute as a senior R&D Engineer. Her research interest mainly focuses on intelligent sensing systems.

Caofeng Pan received his B.S. (2005) and Ph.D. (2010) degrees in Materials Science and Engineering from Tsinghua University. He then joined the Georgia Institute of Technology as a postdoctoral fellow. He has been a professor and a group leader at Beijing Institute of Nanoenergy and Nanosystems, CAS since 2013. His main research interest focuses on the fields of low dimensional materials for fabricating smart electronic and optoelectronic devices for tactile sensing.